SAKARYA ÜNİVERSİTESİ
FEN BİLİMLERİ ENSTİTÜSÜ DERGİSİ

Sakarya University Journal of Science
SAUJS

e-ISSN 2147-835X Period Bimonthly Founded 1997 Publisher Sakarya University
http://www.saujs.sakarya.edu.tr/

Title: Transition Gas Flow Between Two Parallel Plates with a Slit-Type Obstacle of Various Geometry by Event-Driven Molecular Dynamics Simulation

Authors: Mustafa KOÇ, İlyas KANDEMİR, Volkan Ramazan AKKAYA

Recieved: 2022-03-02 00:00:00

Accepted: 2022-06-01 00:00:00

Article Type: Research Article

Volume: 26
Issue: 4
Month: August
Year: 2022
Pages: 720-744

How to cite
Mustafa KOÇ, İlyas KANDEMİR, Volkan Ramazan AKKAYA; (2022), Transition Gas Flow Between Two Parallel Plates with a Slit-Type Obstacle of Various Geometry by Event-Driven Molecular Dynamics Simulation. Sakarya University Journal of Science, 26(4), 720-744, DOI: 10.16984/saufenbilder.1081717
Access link
http://www.saujs.sakarya.edu.tr/en/pub/issue/72361/1081717

Sakarya University Journal of Science 26(4), 720-744, 2022

Transition Gas Flow Between Two Parallel Plates with a Slit-Type Obstacle of Various Geometry by Event-Driven Molecular Dynamics Simulation

Mustafa KOÇ*[1], İlyas KANDEMİR[2], Volkan Ramazan AKKAYA[3]

Abstract

In this study, pressure-driven flow through a slit-type obstacle with various lengths (L) and heights (H) placed in between two parallel plates was investigated by Event-Driven Molecular Dynamics (EDMD) simulation. Mach number, temperature and pressure distributions were obtained along the channel in the transition regime. The change in these macroscopic properties and flow rate were examined for different cases created by changing Knudsen number (Kn) of the flow, the geometry of the slit and the outlet/inlet pressure ratio of the flow. Collision of gas molecules with plates and the obstacle were modeled with diffusive reflection boundary condition. The flow rate showed a sudden change in the transition regime and significant differences in the molecular regime depending on the pressure ratio. Except for the Kn, H and L dimensions were found to be effective in Mach disc formation. Pressure drops at the exit of the slit were shaped differently in normalized pressure profiles depending on Kn, H and L dimensions. In addition, the structure of the vortices formed at the entrance and exit of the slit varies depending on Kn. Some of the results obtained were confirmed to be consistent with similar studies in the literature.

Keywords: Event-Driven Molecular Dynamic Simulation, Knudsen Number, Slit Flow, Mach Discs, Transition Regime, Vorticity.

1. INTRODUCTION

Gas flow due to pressure difference through a slit is one of the major problems in rarefied gas dynamics. Flow through a slit between parallel plates occurs in different technological applications such as spacecraft, micro-propulsion systems, micro nozzle flows, electronic microscopy, MEMS or measurement of sudden and rapid pressure change in vacuum gauges [1-3]. To understand and solve such problems, flow through a narrow section of a channel should be studied. Even small or large pressure differences have significant importance in the design and optimization of various industrial equipment types [4]. Even the rarefied gas flow between two parallel plates of finite length is of practical importance in membrane applications [5].

* Corresponding author: phd.mustafakoc@gmail.com
1 Beykent University, Vocational School, Department of Mechanical and Technologies
ORCID: https://orcid.org/0000-0002-5417-2604
2 Gebze Technical University, Faculty of Aeronautics an d Astronautics
E-mail: kandemir@gtu.edu.tr
ORCID: https://orcid.org/0000-0002-8773-6541
3 Mugla Sıtkı Kocman University, Faculty of Technology, Department of Energy Systems Engineering
E-mail: m.kahyalar@tirsankardan.com.tr
ORCID: https://orcid.org/0000-0002-5052-8554

Rarefied gas flow observed in different technological areas including high altitude and space dynamics [6]. Examination of such flows is characterized by Knudsen number which is a dimensionless parameter defined as ratio of molecular mean free path to the scale of physical domain.

The numerical calculation of high Kn number flow regimes cannot be modeled with the Navier-Stokes equations (N-S), which approach the fluids as a bulk mass movement. For this, the equations based on the Kinetic Theory, which considers the fluid as the motion of the molecular, need to be solved numerically. Molecular simulation models such as Direct Simulation Monte Carlo (DSMC), Lattice Boltzmann (LBM) and Molecular Dynamics (MD) are available for such simulations.

Unlike CFD studies, which rely on solving Navier-Stokes equations, a molecular dynamics (MD) simulation does not require solving a set of differential equations. Instead, it detects and determines the type of each intermolecular interaction, and from these interactions it reveals the entire macroscopic behavior of the flow.

The DSMC method [7] uses several representative molecules to simulate a larger number of real molecules. The movements of the molecules are certain, but the determination of collisions is probabilistic. On the other hand, MD simulations are much more realistic and accurate because each particle represents a real molecule and its position and velocity are known exactly. Due to its time-oriented nature, it contains algorithms suitable for the integration of Newton's equation of motion for many time steps for multi-particle systems. The main disadvantages of standard MD simulations based on the continuous interaction potential (the most widely used being the Lennard-Jones potential) are the limitations in simulation time and size. The computation becomes more difficult as the number of molecules increases, because the interacting particles and their positions must be calculated for each interaction. The integration time step is so small that during a simulation of ten microseconds, even ten thousand molecules representing a very small volume require too many time steps and a collision test at each step.

Thanks to the hard-sphere assumption, where the interaction potential is considered to be discrete (zero except for the moment of contact), collision times can be predicted analytically, allowing the simulation to be treated as asynchronous sequences of events. This is called Event Driven Molecular Dynamics (EDMD) simulations and allows simulation of larger systems for longer periods of time than time-based simulations. It has been shown that this approach produces consistent results in the calculation of transport coefficients for rare gases [8-10]. Unlike in DSMC, molecular trajectories, determination of collision pairs and post-collision velocities are calculated deterministically in EDMD. Also, all collisions are real and predictable, no collision is neglected. Since the first introduction of EDMD simulations [11], the development of more efficient algorithms has further improved the performance of EDMD [8, 12, 13]. With the computing power of a desktop computer, simulation of millions of particles is possible for longer periods [14]. Another advantage of the EDMD method is that it is as deterministic as other classical MD methods and allows working with as many molecules as the DSMC method. Rather than relying on data from a very small number of molecules simulated as in DSMC, it treats all molecules in this physical space as real molecules and all interactions as real interactions, using the entire simulation space as physical space. Thanks to these assumptions and improvements in EDMD, computing performance can compete with DSMC.

LBM, which is a class of CFD, models the liquid as fictitious particles and such particles perform sequential propagation and collision operations on a separate lattice network. LBM solves a simplified version of kinetic equation and does not track each particle as in classical MD. It uses the equation with single particle velocity to simulate fluid flows. Unlike EDMD, the velocity, position and momentum states of the system are calculated probabilistically in the phase space. LBM simulates behavior of fluid flows with macroscopic fluid dynamics of an imaginary ensemble of particles whose motion and interactions are confined to a regular space-time lattice. Particle velocities are constrained by assuming that particles at each location can only

move along a finite number of directions. In addition, slip boundary conditions need to be added to simulate rarefied flow range in LBM. Unlike LBM, all particles are real, and motion and collision detection is calculated by analytical Newton's laws, also it can simulate high Knudsen number rarefied flows without any boundary conditions in EDMD.

Flow properties in a slit connecting reservoirs with two different pressures are studied with DSMC method [15] in the literature. This connection is sometimes a very short pipe and sometimes an infinitely thin border. Since these reservoirs are assumed to be infinitely large, their pressure does not change during the flow. The calculation is made by dividing the slit and the regions close to the slit into small domains. In common results, velocity, number density and temperature undergo a sudden change only in the slit region. These parameters of the molecules that cross the slit come to their states in the upstream region after a certain distance. Briefly reviewing the literature: In the studies of Danilatos [16], Sharipov [17] and [18], Wang and Li [19], Varoutis et al.[5], Argon, Helium and Nitrogen gases were used in a wide range of Kn-related flow regimes, especially in the transition regime, studied the flow through an orifice or slit channel. They investigated the distribution of number and density, velocity, temperature, pressure and flow rates along the flow axis and their variations according to pressure ratios, L/H ratios or only L or H dimensions. Sharipov and Strapasson [20], on the other hand, investigated the same problem with the DSMC method based on ab-initio potential and added krypton to the monoatomic gases. In addition to macroscopic distributions and flow rates, Graur et al. [21] also obtained the velocity profile in the orifice cross-section. But none of them changed the H height. Rahmati and Ehsani [22] obtained streamwise velocity profiles by using LBM method [23] in slip condition. Misdanitis et al. [24] conducted a similar study using the BGK. Pantazis and Valougeorgis [4], who conducted the same flow study, used the BGK model [25] that conforms to the Maxwell specular-diffuse boundary condition. Comparing DSMC simulations with their experimental studies, Gimelshein [26] and Lilly [27] also examined the effect of L geometry and surface interaction on impulse and propulsion. Lindström et al. [28] analyzed the mass flow rate of flow at various pressure ratios and different orifice geometries using a solver based on Navier-Stokes equations. Sharipov [29] calculated mass flow rate, temperature and velocity distributions based on time in transition and steady regime and also evaluated the times when the flow became steady in various regimes. Similarly, Polikarpov and Graur [2] and Ho and Graur [30], who made time-dependent calculations, investigated dependence of time to steady on various parameters in the entire Kn regime. In the study of Varoutis et al. [5], the flow rate between two parallel plates was examined depending on the L/H ratio. However, they did not place any obstacles in the channel. In the literature, molecule-wall interactions are generally modeled as specular or diffuse.

Flow between two parallel plates is in the literature, but the flow through an obstacle between the plates has not been studied yet. Also, the effect of H on the flow together with Kn and outlet/inlet pressure ratio is missing in the literature. Therefore, the macroscopic flow properties of these problems were investigated in this study. EDMD method has been applied for the first time to model such a flow considering all its advantages.

In 2nd section, the calculations and assumptions used for modeling the EDMD simulation will be explained. In 3rd section, the problem of present study will be defined and the setup of the simulation will be mentioned. In 4th section, simulation results will be given together with the validations and the results will be interpreted. Conclusion part and a detailed summary will be given in 5th section.

2. COMPUTATIONAL METHODS OF EDMD SIMULATION

The classical MD method needs a large computational power due to the continuous potential. Monoatomic molecules are modeled as hard-spheres in EDMD. For hard-sphere model, interaction potential between molecules is discrete and only exists in case of contact. Only binary

collisions are considered. No external force field exists, hence the resulting trajectories are linear and molecular velocity between the two collisions is constant. Thus, unlike conventional MD, there is a discrete potential approach instead of a continuous potential. Therefore, molecular trajectories, determination of collision pairs and post-collision velocities can be calculated deterministically in EDMD. Also, all collisions are real and predictable, no collision is neglected.

For the two molecules moving along their trajectories to collide, the contact condition must be met:

$$\sum_{k=1}^{3}\left(x_{j,k}^{*}-x_{i,k}^{*}\right)^{2}=\frac{\left(d_{m,j}+d_{m,i}\right)^{2}}{4} \tag{1}$$

Here i and j denote the pair of the molecules to collide, x_k^* position component, d is diameter of the molecules. The positions of the molecules when the collision occurs are calculated from the following formula:

$$\begin{aligned} x_{i,k}^{*} &= x_{i,k}+c_{i,k}(t-t_i) \\ x_{j,k}^{*} &= x_{j,k}+c_{j,k}\left(t-t_j\right) \end{aligned} \tag{2}$$

where c_k is velocity component, t_i and t_j are separate time variable held for each molecule. If Eq. (1) is substituted in Eq. (2), the following is obtained.

$$\begin{aligned} \sum_{k=1}^{3}\Big(x_{i,k}+c_{i,k}(t-t_i)-x_{j,k} \\ -c_{j,k}\left(t-t_j\right)\Big)^{2}=d^{2} \end{aligned} \tag{3}$$

To get a simpler form of Eq. (3), Δx_k and Δc_k are defined:

$$\begin{aligned} \Delta x_k &= c_{j,k}\Delta t_{i,j}+x_{j,k}-x_{i,k} \\ \Delta c_k &= c_{j,k}-c_{i,k} \end{aligned} \tag{4}$$

Hence, Eq. (4) would be as follows:

$$\begin{aligned} \sum_{k=1}^{3}(\Delta c_k)^2(t-t_i)^2+2\Delta x_k\Delta c_k(t-t_i) \\ +(\Delta x_k)^2=d^2 \end{aligned} \tag{5}$$

For a simpler representation $A=\sum_{k=1}^{3}(\Delta c_k)^2$, $B=\sum_{k=1}^{3}\Delta x_k\Delta c_k$ and $C=\sum_{k=1}^{3}(\Delta x_k)^2-d^2$ are defined. So, the collision time becomes the following quadratic form:

$$A(t-t_i)^2+2B(t-t_i)+C=0 \tag{6}$$

In case of no real roots, the trajectories do not intersect. If positive real roots exist, the smallest one gives the collision time. This allows one to estimate the collision times deterministically. Thus, the simulation consists of a series of asynchronous events. Due to its event-driven nature, time can advance discretely from one event to subsequent one in simulation.

On the initialization, thermal equilibrium is assured for for entire domain after a certain amount of time. Since monoatomic molecules have only translation energy mode, relationship between the kinetic temperatures and the average translational kinetic energies of molecules in thermal equilibrium is given as:

$$\frac{3}{2}k_bT=\frac{1}{2}m\langle c^2\rangle \tag{7}$$

Here $\langle c^2\rangle$ is the average of thermal velocity squares of molecules. According to Kinetic Theory, the velocities of molecules in a system at thermal equilibrium are sampled from the Boltzmann distribution. The most probable speed according to this distribution is as follows.

$$c_{mp}=\sqrt{\frac{2}{3}\langle c^2\rangle} \tag{8}$$

Thus, the thermal velocity components sampled from the distribution are as follows.

$$u_{th} = c_{mp}\sqrt{-ln(R_1)}\,sin(2\pi R_2)$$
$$v_{th} = c_{mp}\sqrt{-ln(R_3)}\,sin(2\pi R_4) \quad (9)$$
$$w_{th} = c_{mp}\sqrt{-ln(R_5)}\,sin(2\pi R_6)$$

When a collision occurs, post-collision velocities are determined analytically by conservation of energy and momentum. The type of molecule pair that participates in the collision determines the collision characteristic. Since intermolecular collisions are elastic, mass, translational energy, and momentum are conserved.

$$m_A + m_B = m'_A + m'_B$$
$$m_A c_A + m_B c_B = m'_A c'_A + m'_A c'_B \quad (10)$$
$$m_A|c_A|^2 + m_B|c_B|^2 = m'_A|c'_A|^2 + m'_A|c'_B|^2$$

Here $'$ indicates post-collision state. m and c indicate mass and velocity vector of the molecule, respectively. Accordingly, the post-collision velocities of the molecule pair are expressed as follows.

$$c'_A = c_A - \frac{2\mu_{AB}}{m_A}\epsilon\langle\epsilon, c_A - c_B\rangle$$
$$c'_B = c_B - \frac{2\mu_{AB}}{m_A}\epsilon\langle\epsilon, c_A - c_B\rangle \quad (11)$$

Here the inner product is shown as$\langle\cdot,\cdot\rangle$. μ_{AB} is reduced mass and ϵ is the unit vector passing through the molecule centers when two molecules are in contact.

$$\mu_{AB} = \frac{m_A m_B}{m_A + m_B}$$
$$\epsilon = \frac{x_A - x_B}{|x_A - x_B|} \quad (12)$$

Generally, three types of computational domain boundary models are considered sufficient to model a flow in micro- and nano-channels. These are periodicity, wall interaction and flow boundary conditions. In the presence of periodic boundaries simulation domain is modelled as an infinite lattice by repeating the calculation region along the boundary direction. When a molecule physically crosses a periodic boundary, it leaves the computational domain and enters the opposite boundary at the same velocity components. As a result of specular reflection of a molecule, the tangential velocity components remain the same while the normal velocity component, which conserves the tangential momentum, is reversed. In real life, the wall surface is rough, and molecules are projected at random angles from the wall. Diffuse reflection is the most common model representing these surfaces. The post-collision velocity of the molecule is largely independent of the incoming velocity and is stochastically determined from a distribution based on wall temperature (T_W).

Molecules reaching both ends of the system (upstream or downstream) leave the computational domain permanently. New molecules are inserted into the computational domain according to local domain properties. For both flow boundaries, the molecular flux entering the calculation domain is determined by the Maxwell distribution function:

$$F_j = \frac{n_j}{2\sqrt{\pi\beta_j}}\left[\begin{matrix} e^{-s_j^2 cos^2\phi} + \\ \sqrt{\pi}s_j cos\,\phi\left(1 + erf\left(s_j cos\,\phi\right)\right)\end{matrix}\right] \quad (13)$$

where $s_j = U_j\beta_j$, $\beta_j = 1/c_{mp,j} = 1/\sqrt{2k_bT_j\,/\,m}$. Here, U, T, n_j and c_{mp} are streamwise velocity, local temperature, number density of molecules in the cell and the most probable speed, respectively. This molecular flux should be calculated for each cell surface of each flow boundary cell j. The value of ϕ is 0 for upstream and π for downstream. The number of molecules entering the calculation domain from the cross-sectional area (A) of the boundary surface per unit time (Δt) gives the following relation:

$$N_{in,j} = F_j\Delta t A_j \quad (14)$$

The tangential velocity components (v and w) of the incoming molecules that are independent of streamwise are produced as follows:

$$v = V + c_{mp}\frac{R_n}{\sqrt{2}}$$
$$w = W + c_{mp}\frac{R'_n}{\sqrt{2}} \quad (15)$$

Here, V and W are mean tangential velocity components, and R_n and R'_n are randomly generated numbers from a normal distribution with zero mean and unit variance.

When the streamwise velocity (U) is zero, normal component is expressed as:

$$u = c_{mp}\sqrt{-logR_u} \quad (16)$$

Here, R_u is random number generated from uniform distribution of interval [0,1). For $U \neq 0$, Garcia and Wagner [31] introduce several efficient acceptance-rejection methods with the general form:

$$u = U - f\left(\frac{U}{c_{mp}}\right)c_{mp} \quad (17)$$

Here, $f(U/c_{mp})$ is a randomly selected number from the acceptance-rejection method. In this study, recommended method for low-speed flows ($-0.4c_{mp} < U < 1.3c_{mp}$) was used.

The inlet pressure (p_{in}) and temperature (T_{in}) are known for the upstream boundary. V_{in} and W_{in} are set to zero. The molecular number density is calculated from the ideal gas equation:

$$n_{in} = \frac{p_{in}}{k_b T_{in}} \quad (18)$$

Streamwise velocity perpendicular to the surface is expressed as a function of the mean flow velocity (U_j), pressure (p_j), density (ρ_j) and sound velocity (a_j) of the computational domain:

$$(U_{in})_j = U_j + \frac{p_{in} - p_j}{\rho_j a_j} \quad (19)$$

Only the outlet pressure (p_e) is known at the downstream boundary. Other flow properties are calculated by extrapolating from neighboring cell:

$$(n_e)_j = n_j + \frac{p_e - p_j}{(a_j)^2}$$
$$(U_e)_j = U_j + \frac{p_j - p_e}{\rho_j a_j} \quad (20)$$
$$(T_e)_j = -\frac{p_e}{(n_e)_j k_b}$$

The tangential components of the average flow velocity components are calculated similarly for the upstream:

$$(V_e)_j = V_j$$
$$(W_e)_j = W_j \quad (21)$$

No macroscopic information, except for the initial conditions and boundary conditions, is imposed on the system in EDMD simulations. Defining the fluid as an ensemble of molecules allows all macroscopic features of the system to be calculated from the instantaneous velocity, position and energy information of each molecule. The number of molecules inserted into the calculation domain from the flow boundary and their respective velocities are calculated by means of local flow properties such as temperature, pressure, molecular density and average velocity.

In the pioneering work of this study [10], Event-Driven Molecular Dynamic Simulation (EDMD) model to simulate rarefied gas flow was developed with Object-Oriented C# programming in Visual Studio. In order to reduce computational complexity of EDMD simulation, a cell division method [8] was used. In this method, each molecule is placed in a cell according to its position and a cell has 27 neighbor cells in 3D. For an intermolecular collision, the distance between two molecules must be less than the width of the cell. So they have to cross the cell border before they collide. So that only molecules of the same or neighboring cells are possible collision candidates at a given time, and it is unnecessary to check

whole computational domain. No collision is missed thanks to this multi-cell method. The simulation aims to find the earliest event and to process it. For this, the priority queue method [32], [33] is implemented in EDMD by Akkaya and Kandemir [10] and reduces the computational complexity to *O*(logN). For data reduction, the calculation domain was divided into small sub-domains (bins) and the average of the snapshots of these bins at a certain time intervals were taken. The implicit treatment method (IBT) for flow boundary is first introduced for DSMC simulations by Liou and Fang [34] and adapted for present EDMD simulations by Akkaya and Kandemir [10]. After implementing the necessary boundary conditions, shear-driven and pressure-driven flow were simulated. In the next development, flow through the porous media modeled with spherical particles and at various porosities was simulated in the transition flow regime [35]. In this study, the problem mentioned in 3rd section was investigated and the simulation was modeled for different cases.

3. PROBLEM DEFINITION AND SETUP OF EDMD SIMULATION

This study focuses on rarefied gas flow through a slit-type obstacle between two parallel plates. The effect of various slit size and inlet/outlet pressure ratio on flow properties are examined in numerous cases. The lower and upper plates and the slit between them, slit gap H and slit length L are shown in Figure 1. L/H has been taken into account while creating different cases for the slit geometry. $L/H = 0$ means L is zero regardless of H. $L/H = 2$ means that L is 2 times H regardless of H. In addition, the effect of separate dimensions of L and H were examined. Entire channel volume is computational domain. The gas pressure p_{in} and temperature T_{in} at the channel inlet and the pressure p_{out} and temperature T_{out} at the outlet are assigned when the simulation is initialized. The temperature of the lower and upper plates and the temperature inside the channel is $300K$ initially. Wall temperature is constant throughout the simulation, but the temperature of the channel is developed due to expansion throughout the simulation. Monatomic Argon gas has been selected as the working fluid. Total number of simulated molecules is 200000. All molecule-wall collisions were modeled as diffuse reflection.

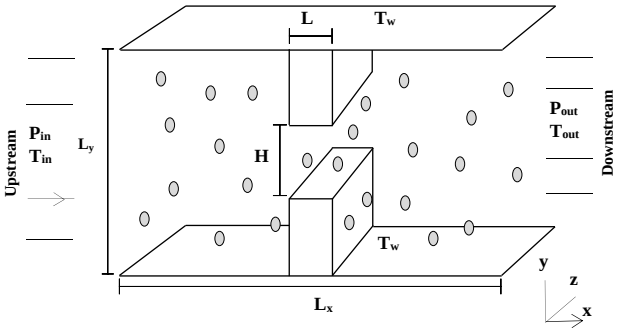

Figure 1. Geometry of computation domain slit and location of slit

While calculating the distribution of macroscopic properties, the channel was divided into 51 regions (bins) in the x − y plane. All 1D distributions are obtained along the channel mid-line in the x-axis by averaging the y and z axes. The properties within each bin were averaged along the z-axis for 2D data. In order to minimize numerical error, non-dimensionalization have been applied by scaling magnitudes with Boltzmann constant k_B=1.38×10^{-23}, reference mass $m = 1.5 \times 10^{-27}$kg and diameter $d = 0.5 \times 10^{-10}$m. Therefore, length of plates is $L_x = 10000 \times d$ and distance between them is L_y =5000× d. Since the z-axis is periodic, the width of the plates is infinite. The local Mach number is calculated with the local root mean square velocity (c_{rms}) and the temperature (T). The macroscopic properties have been calculated for each bin. For the purpose of qualitative comparison, Mach number (M), velocity (u_x), temperature (T), pressure (p) and density (n) distributions in all simulations have been nondimensionalized by normalizing with $2.5M$, $540m/s$, $330K$, $8\times10^6 Pa$ and $2.26\times10^6 m^{-3}$, respectively. Different pressure ratios and Kn are selected for different simulation setups. The slit is placed at position 0.16 L_x to take into account the fluid behavior at the slit entrance and also to follow the behavior at the slit exit to a certain distance.

Pressures at the inlet and inside the channel are initially same. In order to prevent molecule accumulation at the inlet and to obtain a steady flow rapidly, flow is created by applying low pressure only at the channel outlet.

At the initialization, the molecules have been randomly distributed into the channel according to the given pressure and number density. Their velocities are randomly assigned from a distribution function with respect to initial temperature. Specular reflection boundary condition has been valid for channel walls and no slit has been present. Thus, molecules have been allowed to collide enough to reach thermal equilibrium. Then a slit of the desired geometry has been created at the specified location of the channel and the corresponding reflection boundary conditions have been applied to the channel walls (diffusive in the y-axis and periodic in the z-axis). Finally, the pressure boundary condition has been applied to the downstream flows along the x-axis.

To calculate the flow rate ($\dot{m}$), the number of molecules entering (N_{in}) and leaving (N_{out}) the slit of width L are counted in a certain time period (Δt) and m_{mol} is the mass of a single molecule.

$$\dot{m} = \frac{N_{out} + N_{in}}{2\Delta t} m_{mol} \tag{22}$$

Flow rate and macroscopic properties were obtained at different Knudsen numbers (Kn) which can be described as the ratio of molecule's mean free path (λ) to the characteristic length (L_y).

$$Kn = \frac{\lambda}{L_y} \tag{23}$$

Since the H height is a control parameter in this study, it will not be appropriate to use it in Kn calculation. Therefore, Kn was calculated through L_y (channel length). In this way, the effect of the height H on the flow could be examined independently of Kn.

For each simulation, the pressure and density distributions are normalized to their values at the channel inlet. Hence, qualitative comparison of the results has been possible in different Kn, in other words, in density.

4. RESULTS AND DISCUSSION

In the flow rates were obtained according to Kn of transition regime at pressure ratios (p_o/p_i)=0.1 and 0.5 for L/H=0 (L=0) - H=500 and L/H=2 (L=1000) - H=500. As Kn is changing from 0.04 to 10, flow rate decreases. As Kn increases, the flow rate is almost constant until the transition regime. After that, a sudden decrease is observed in mass flow rate. This behaviour remains throughout the transition regime. In the molecular flow regime, it is almost constant. When the pressure ratio (p_o/p_i) increases from 0.1 to 0.5, the flow rate also decreases. This difference in flow rate due to pressure rate is not constant over the entire Kn range. It increases towards the molecular regime and decreases towards the continuum regime. L/H ratio also affects the flow rate. Increasing L creates a thin channel in the slit. This not only causes a decrease in the flow rate for the entire transition regime, but also changes Kn of the transition regime. As L increases, this range shifts towards smaller Kn values. Similar results at low Kn were observed in some DSMC studies [36] with a fixed H height and without top and bottom plates. The effect that creates the difference in high Kn is the increase of momentum transfer between individual molecules and upper and lower plate walls.

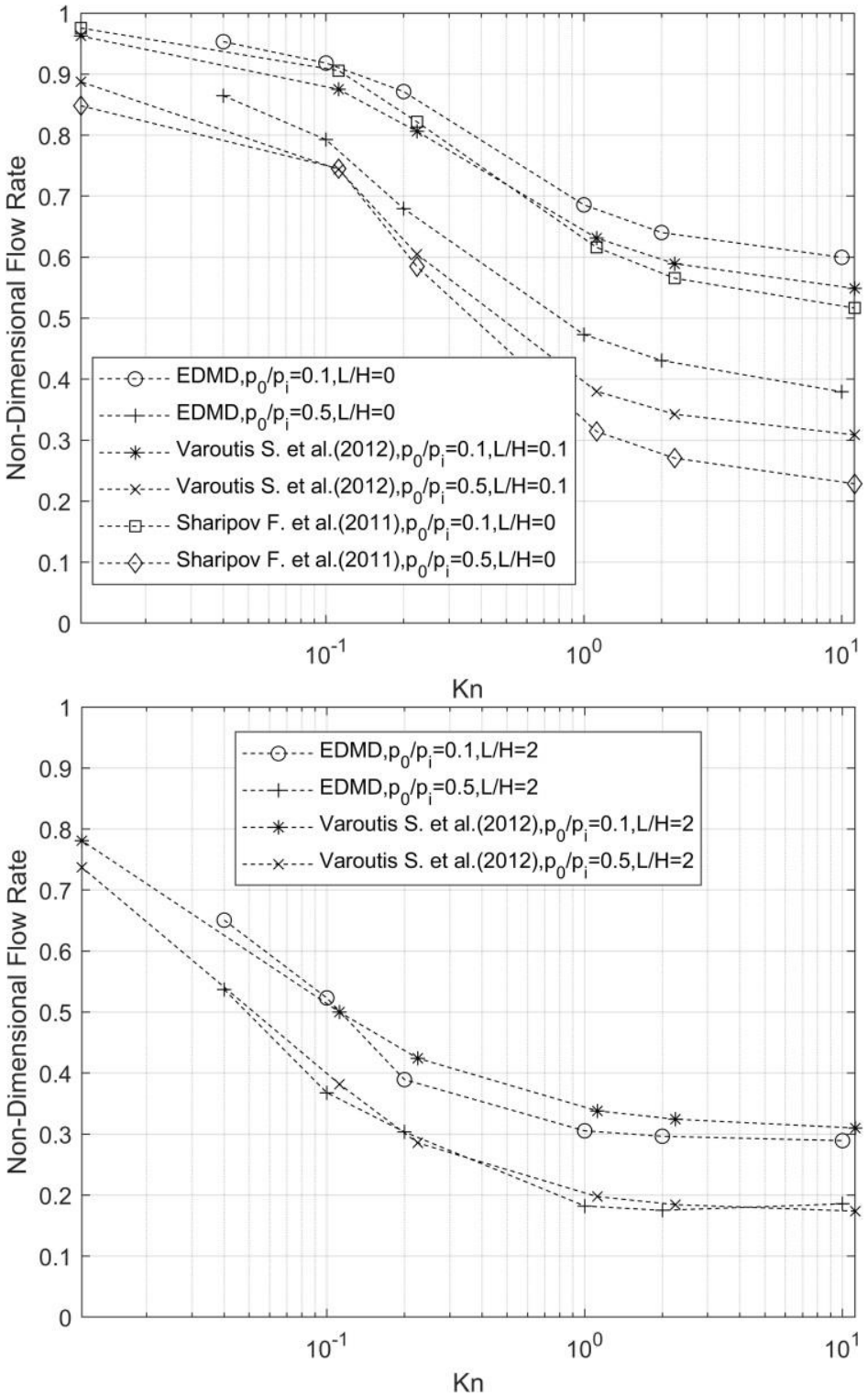

Figure 2 *Kn* vs. Non-Dimensional Flow Rate. p_o/p_i = 0.1 and 0.5 were compared for *L/H*=0(top) and 2(below).

In Figure 3, Mach number (M), temperature (T) and pressure (p) distribution along x/L_x were obtained under flow conditions p_o/p_i=0.1 and 0.5, H=500 and L=0 at Kn in transition regime. As Kn approaches to the continuous regime, the velocity at the slit outlet increases. While the temperature approaches to the initial value towards the channel outlet in low Kn, it decreases further (lower than the initial value) in high Kn. In steady-state flows, a sudden pressure drop is expected at the slit outlet due to the increase in

cross-sectional area. But as the Kn increases, this behavior disappears.

Mach number (M), temperature (T), pressure (p), density (n) contour plots and streamlines of the flow case in Figure 3 are shown in Figure 4 and 5, respectively. At low Kn, more pronounced vortex formations are noticeable at the slit outlet. There are even backflow vortex at the inlet of the slit due to the slit wall obstacle. As Kn increases, the vortex decreases at the slit outlet and begins to form at the slit inlet. For the case of H=500, Mach disk structure did not occur due to the maximum critical M being 0.7 at the outlet of the slit.

p_o/p_i=0.1, H=500 and L=0

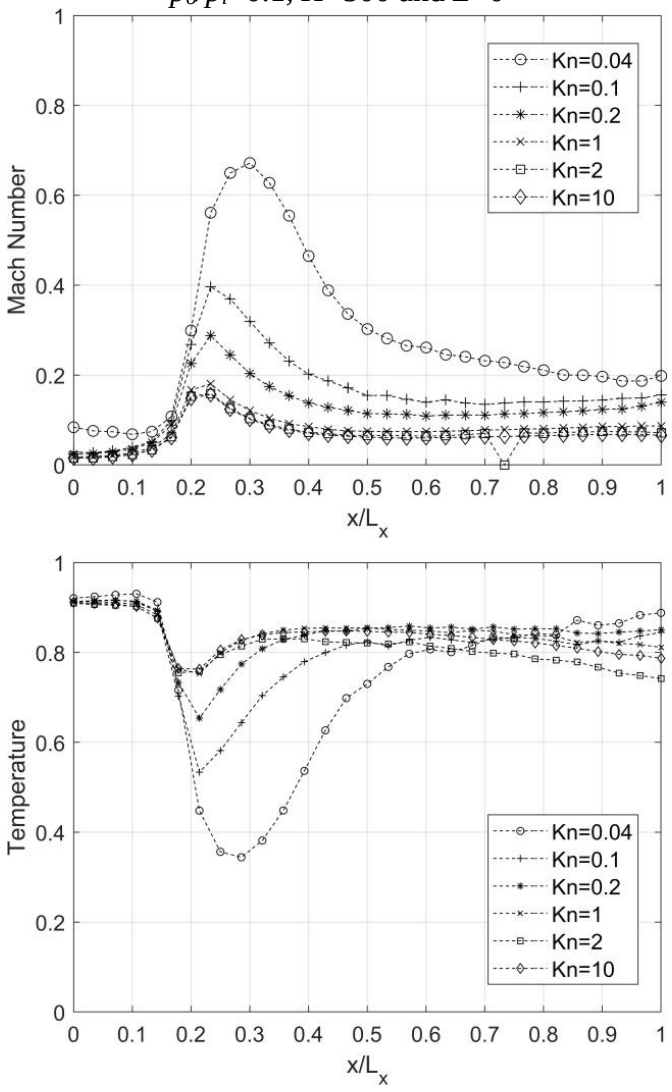

p_o/p_i=0.5, H=500 and L=0

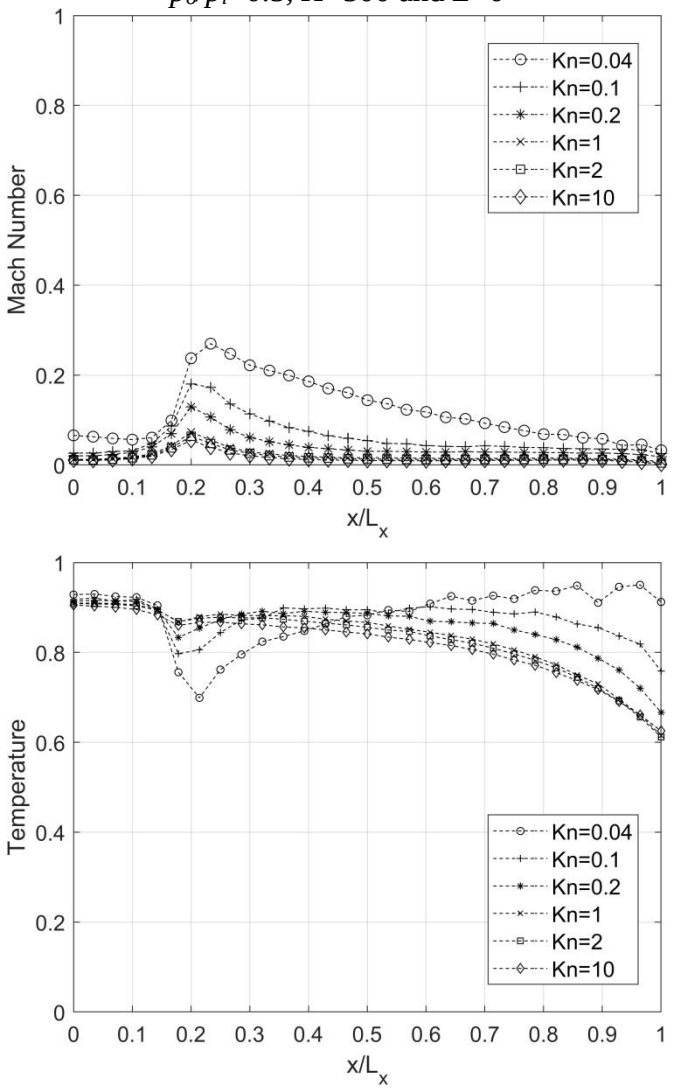

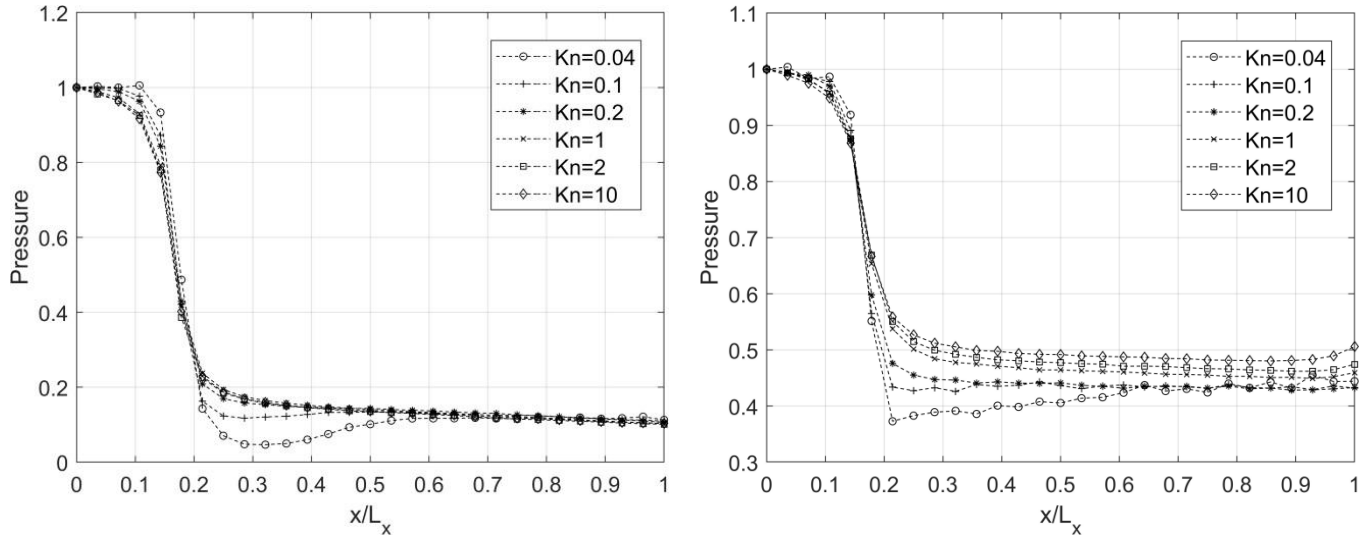

Figure 3 *M*, *T* and *p* distributions along L_x depending on *Kn*. Flow conditions are p_o/p_i=0.1(left) and p_o/p_i=0.5(right), *H*=500 and *L*=0.

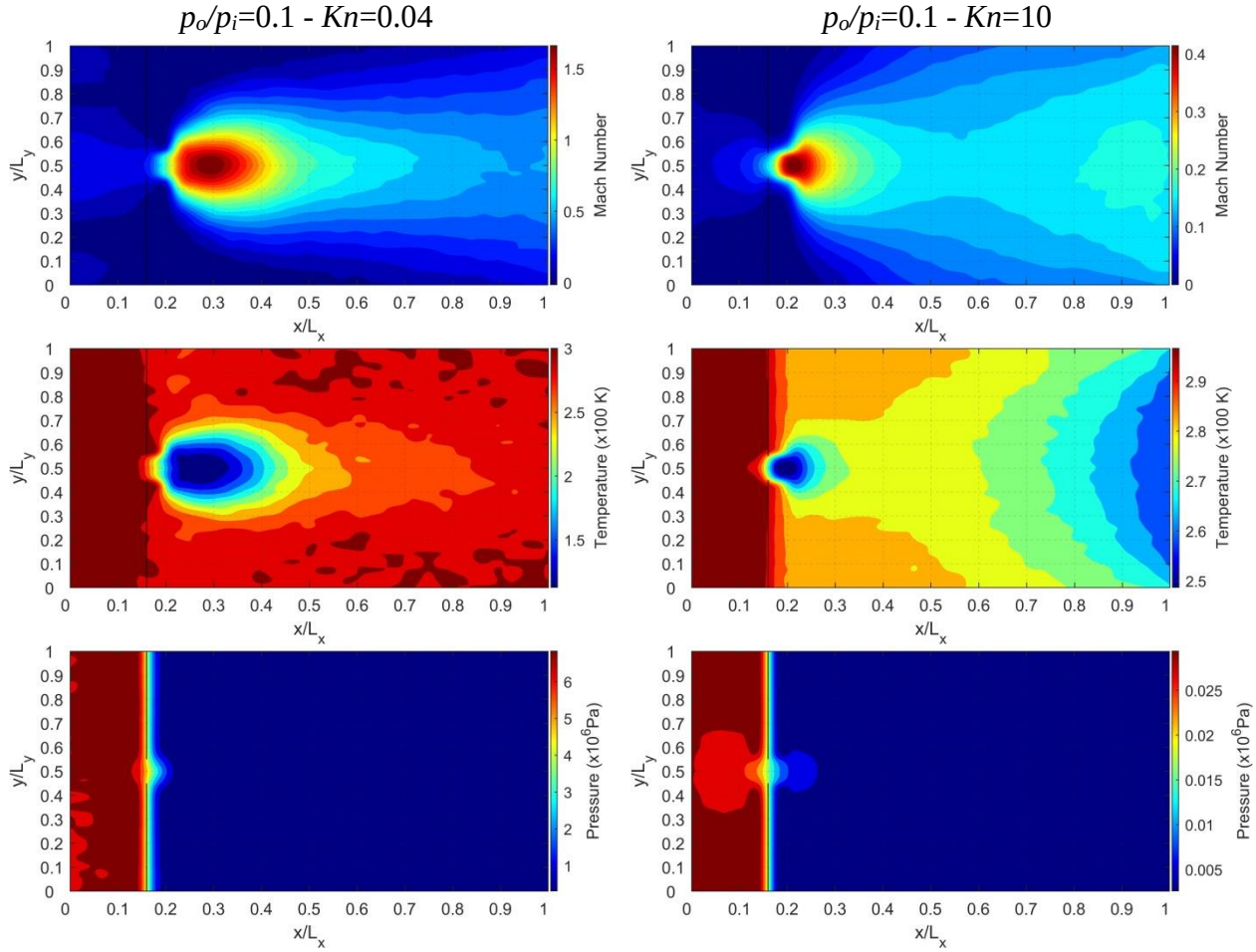

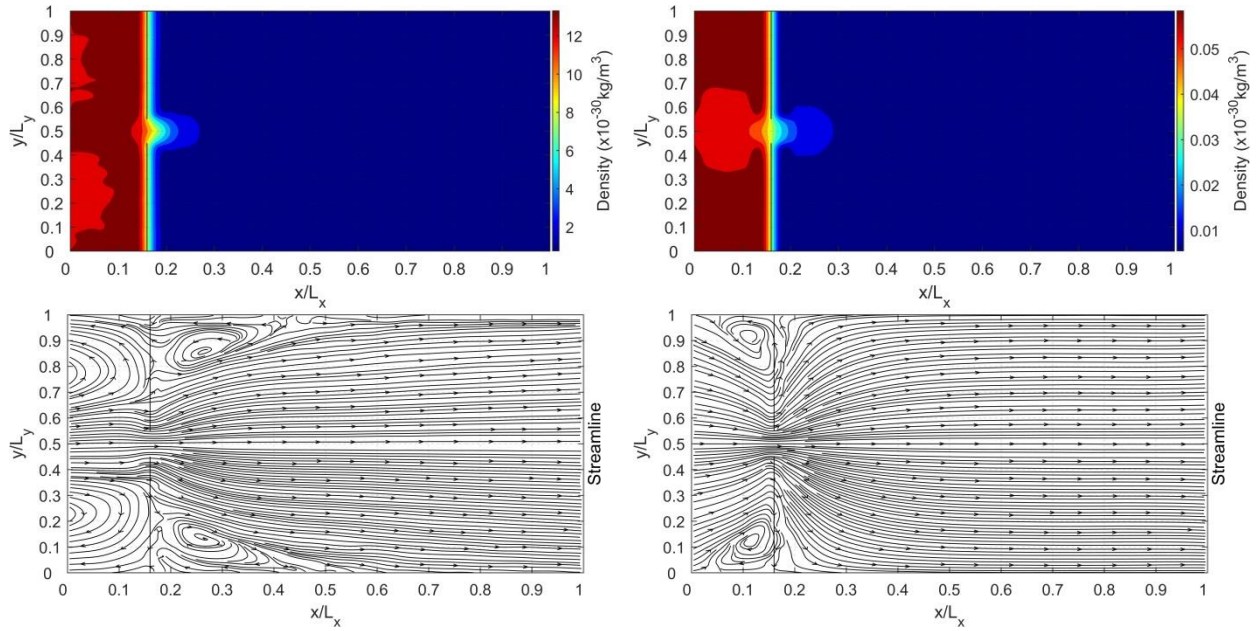

Figure 4 Contour plots of mach number, temperature, pressure, density and streamline. For H=500 - L=0: p_o/p_i=0.1 - Kn=0.04(Left Column), p_o/p_i=0.1 - Kn=10(Right Column).

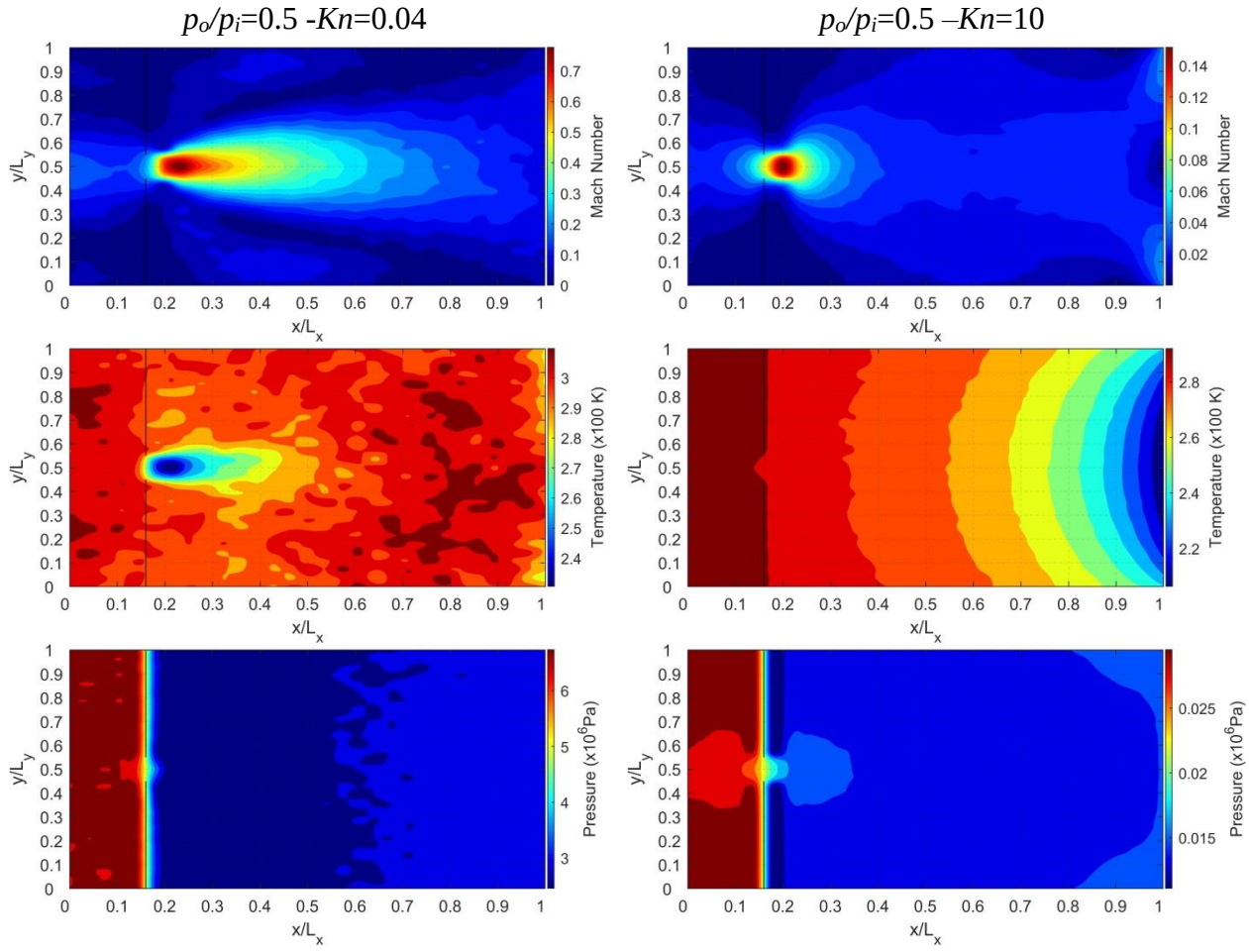

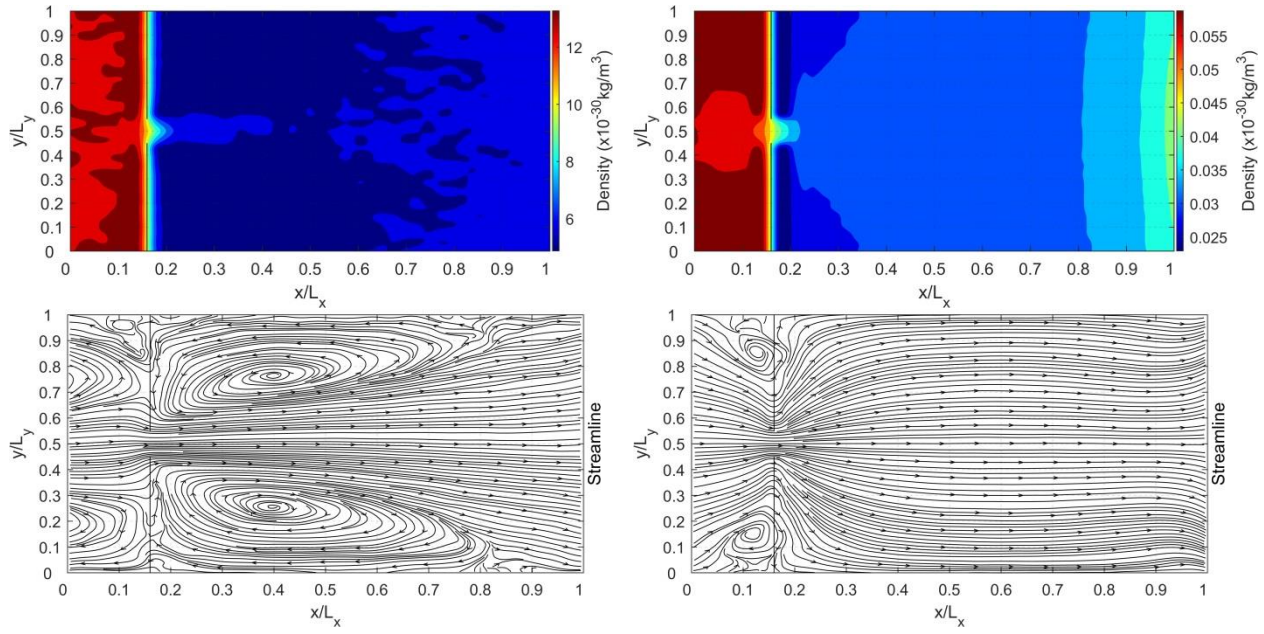

Figure 5 Contour plots of mach number, temperature, pressure, density and streamline. For H=500 - L=0: p_o/p_i=0.5 - Kn=0.04(Left Column), p_o/p_i=0.5 - Kn=10(Right Column).

In Figure 6, Mach number (M), temperature (T) and pressure (p) distributions are presented along x/L_x of the channel at Kn in transition regime for p_o/p_i=0.1 and 0.5, H=1000 and L=0. When the pressure ratio increases 5 times, Mach number doubles at the slit exit for Kn=0.04. Mach number is nearly 1 at the slit outlet. The midline distribution of Mach, temperature and pressure shows more dramatic changes than H=500 at outlet of the slit. Pressure drop at outlet of the slit in case of at H=1000 and p_o/p_i=0.5 for Kn =0.04 is more than H=500 but not valid for p_o/p_i=0.1. In addition, vortices size at outlet of slit in the case of H=500 is smaller than H=1000 especially for lower pressure ratio p_o/p_i=0.5.

p_o/p_i=0.1, H=1000 and L=0

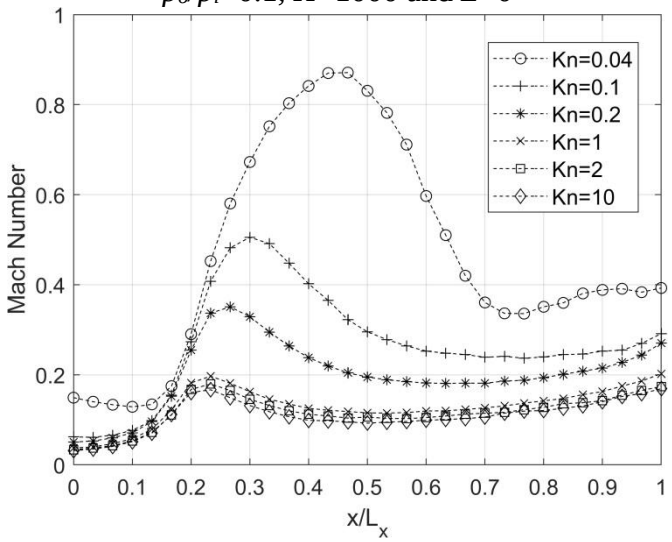

p_o/p_i=0.5, H=1000 and L=0

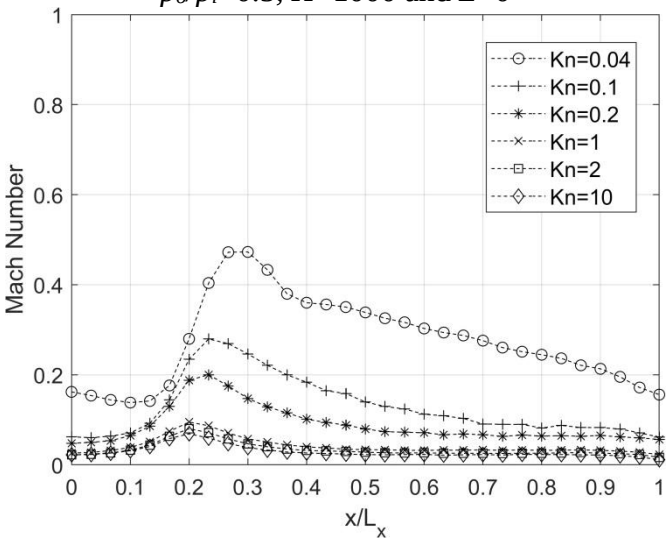

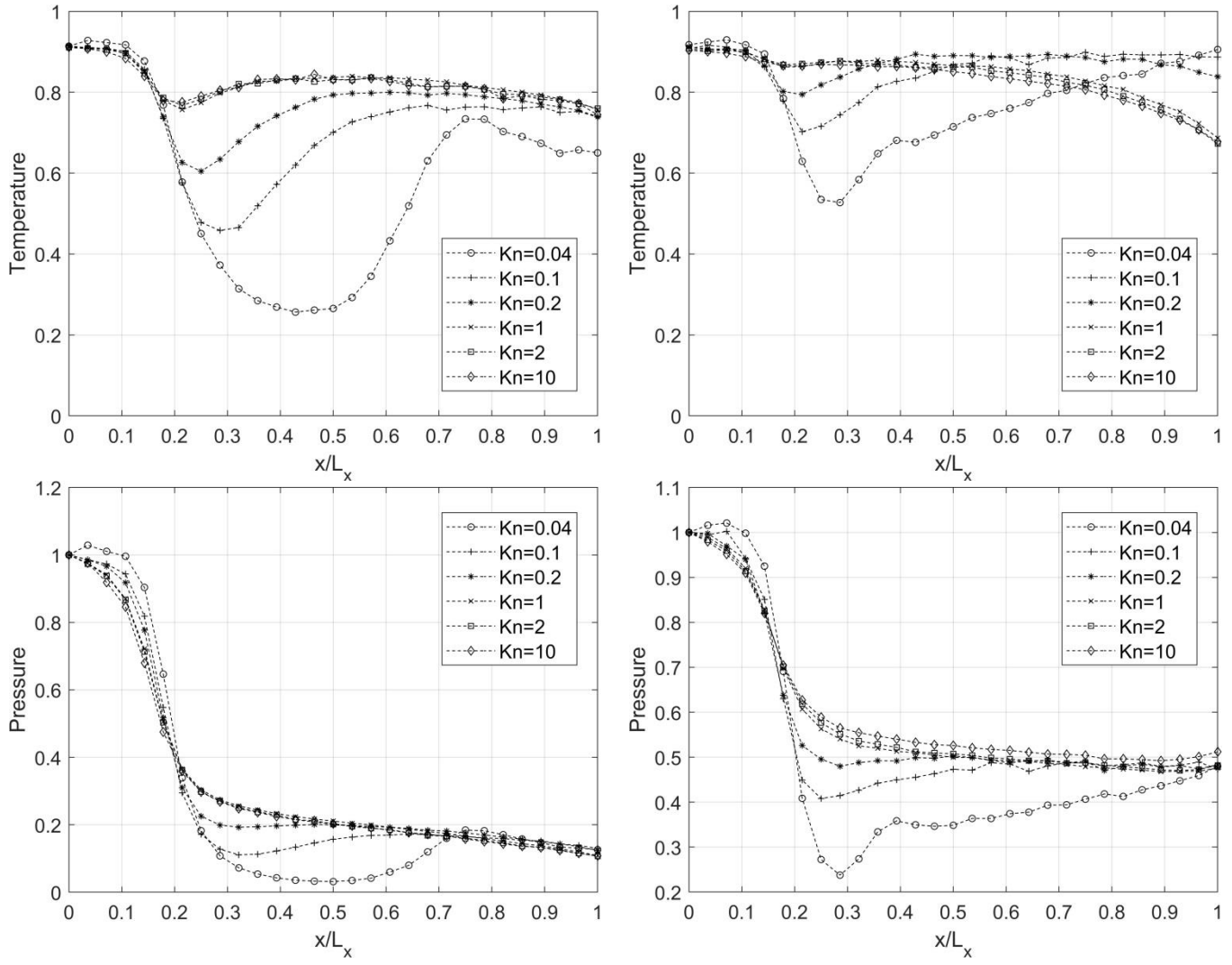

Figure 6 *M*, *T* and *p* distributions along L_x depending on *Kn*. Flow conditions are p_o/p_i=0.1(left) and p_o/p_i=0.5(right), *H*=1000 and *L*=0.

Mach number (M), temperature (T), pressure (p), density (n) contour plots and streamlines of the flow case in Figure 6 are shown in Figure 7 and 8, respectively. Mach discs started to be seen around x=0.75-0.8 at Kn=0.04. Mach disks are characterized by sudden fluctuations in Mach number, velocity, pressure, temperature and density distributions. At the outlet of the slit, a zone of silence is formed, where there is a sudden decrease in pressure and temperature, and a sudden increase in velocity. Then a normal shock occurs by decreasing the velocity. With this, there is a sudden increase in pressure and temperature. The silence zone and normal shock are delimited by the barrel shock. The flow re-thermalizes and is of relatively high density. It has a slightly supersonic flow rate. Flow slows down after barrel shock [21, 37]. Only enlargement of the H dimension caused this. This effect can also be seen in the changes in the x-axis in Figure 6. In the literature, the main factors in the formation of these discs are given as pressure ratio and Kn. Due to the effect of the simulation on the calculation power, only one Mach disc could be seen, since the length of the channel after the slit could not be extended too much and the Kn could not be further reduced. According to the pressure distribution along the channel, the sudden pressure drop at the slot outlet was smaller and farther than the H=500. Thus, it has been revealed that a certain distance is required for the formation of barrel shocks.

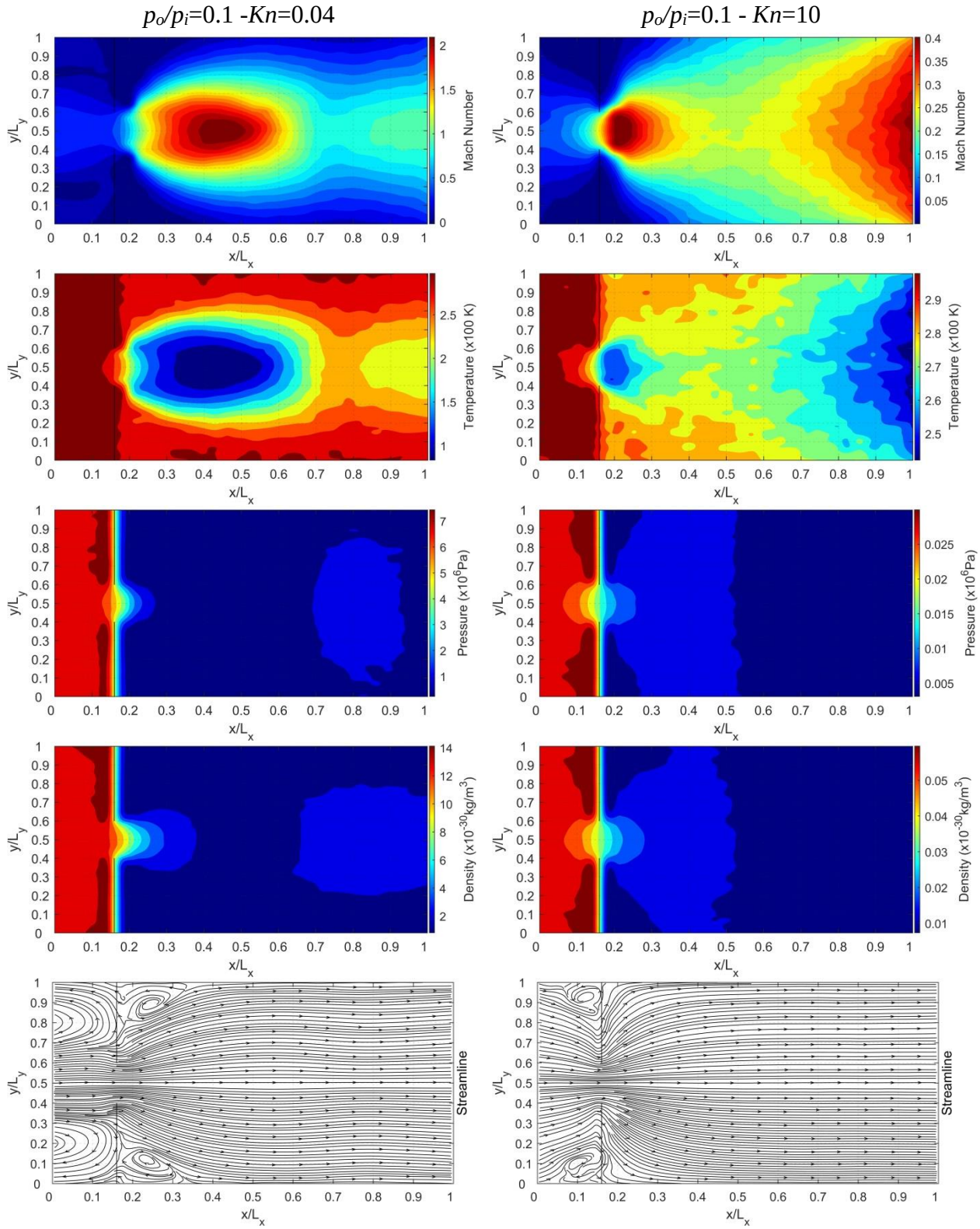

Figure 7 Contour plots of mach number, temperature, pressure, density and streamline. For H=1000 - L=0: p_o/p_i=0.1 - Kn=0.04(Left Column), p_o/p_i=0.1 - Kn=10(Right Column).

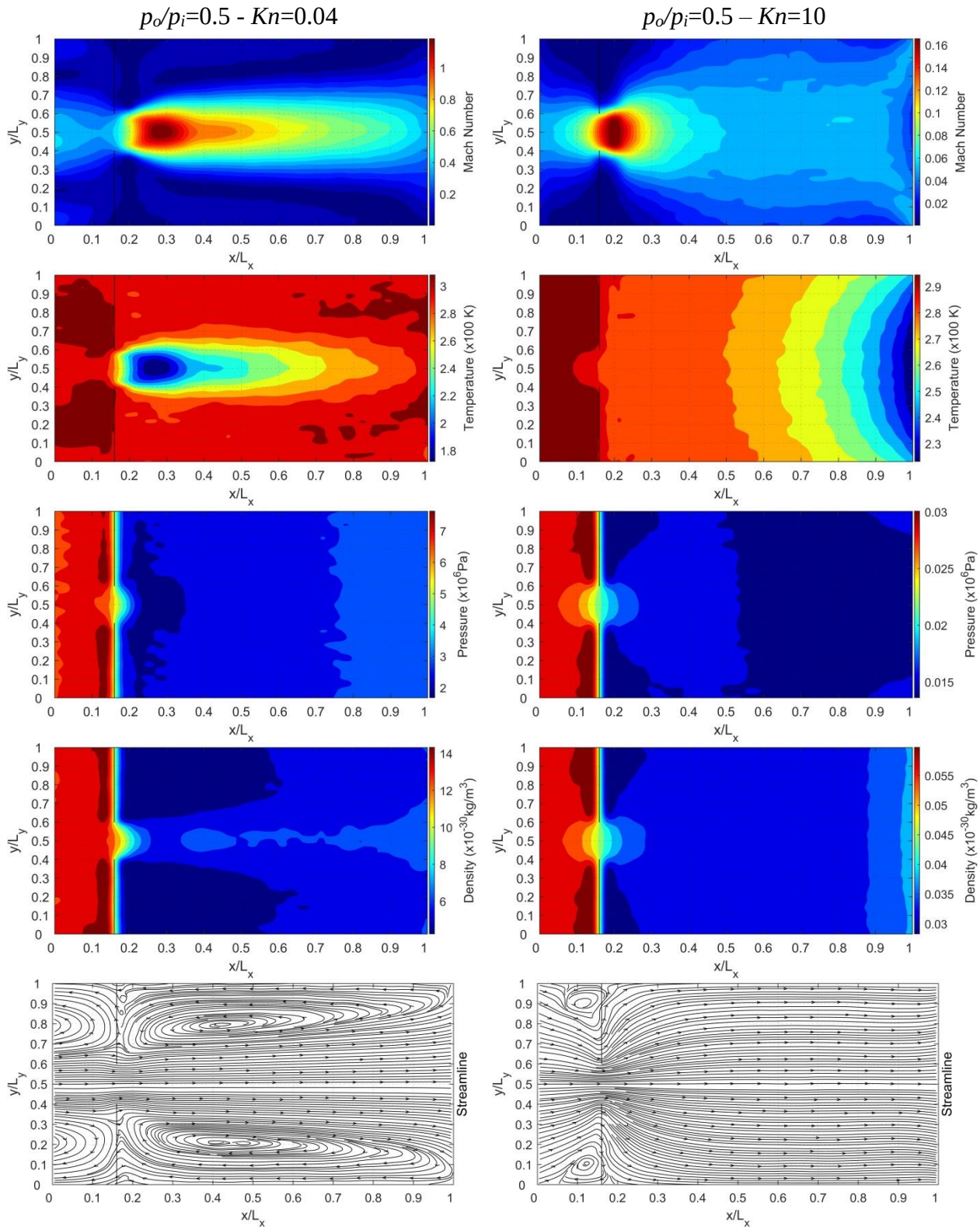

Figure 8 Contour plots of mach number, temperature, pressure, density and streamline. For H=1000 - L=0: p_o/p_i=0.5 - Kn=0.04(Left Column), p_o/p_i=0.5 - Kn=10(Right Column).

In Figure 9, Mach number (M), temperature (T) and pressure (p) changes along x/L_x for different Kn and p_o/p_i=0.1 and 0.5, H=500 and L=1000. Increasing L decreases Mach number at the slit exit. However, it causes vortex formation after the slit to spread longer along the x-axis. The pressure drop at the slit exit was smaller than that of L=0 for the same H. Mach number (M), temperature (T), pressure (p), density (n) contour plots and

streamlines of the flow case in Figure 9 are shown in Figure 10 and 11, respectively.

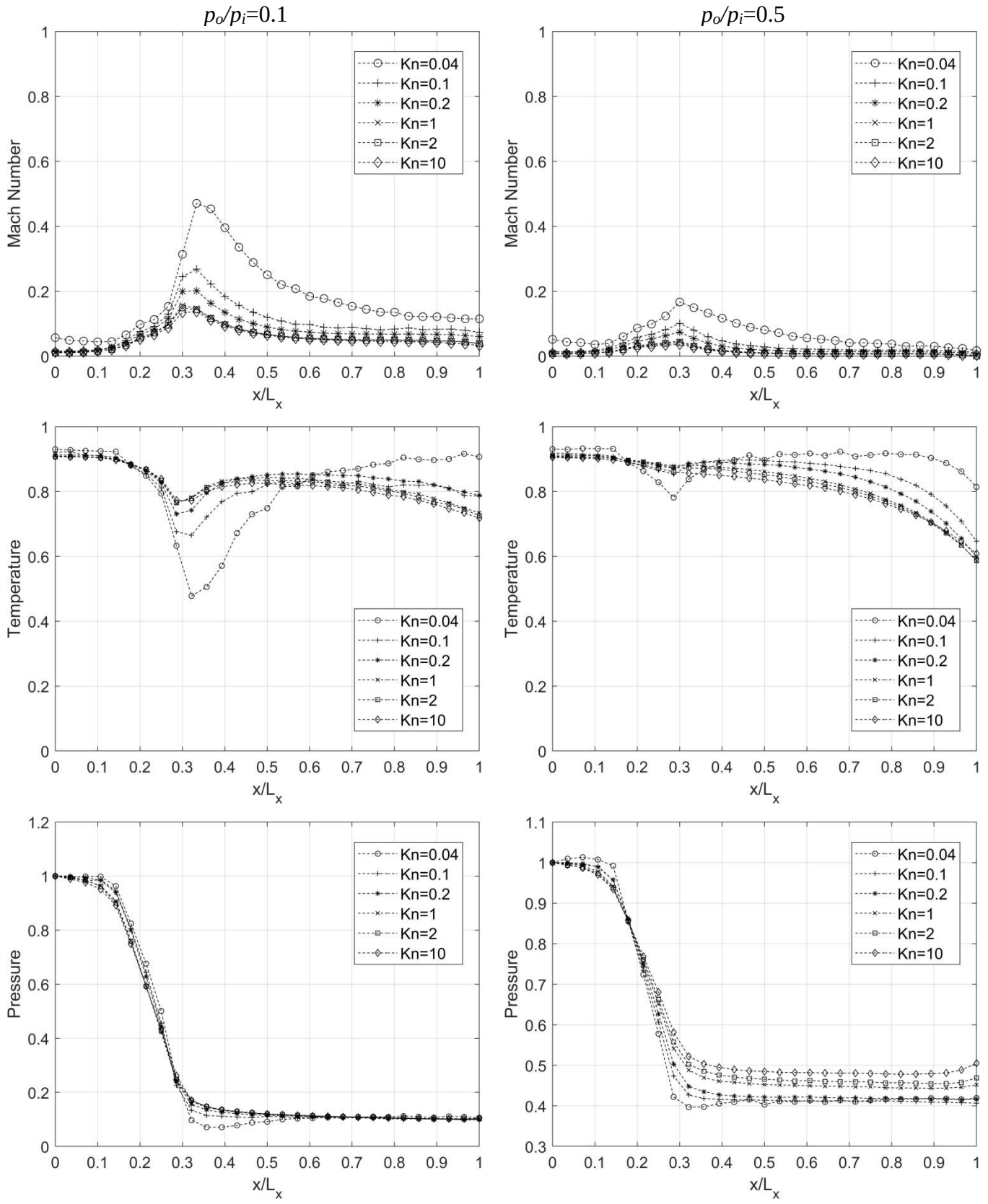

Figure 9 M, T and p distributions along L_x depending on Kn. Flow conditions are p_o/p_i=0.1(left) and p_o/p_i=0.5(right), H=500 and L=1000.

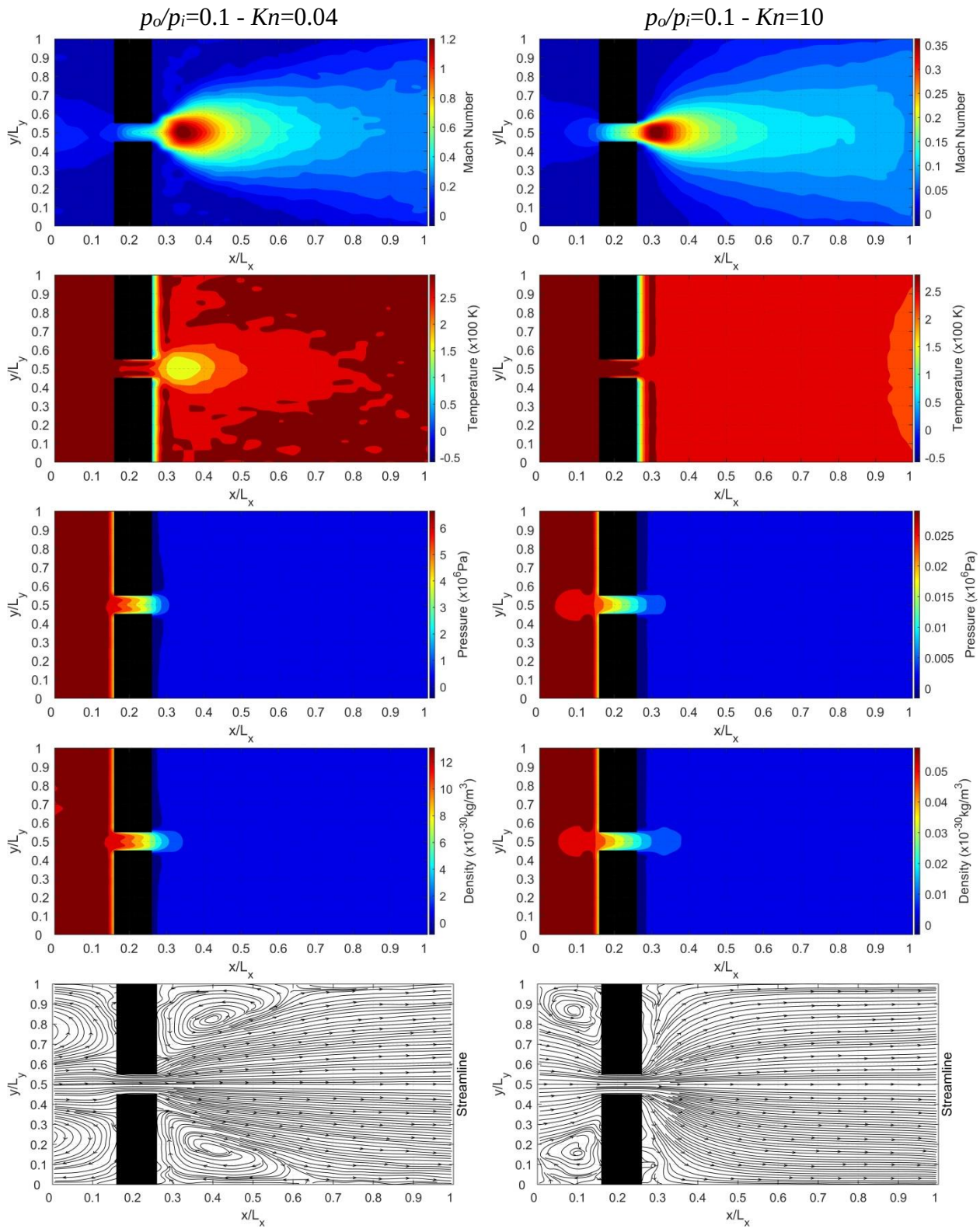

Figure 10 Contour plots of Mach number, Temperature, pressure, density and streamline. For H=500 - L=1000: p_o/p_i=0.1 - Kn=0.04(Left Column), p_o/p_i=0.1 - Kn=10(Right Column).

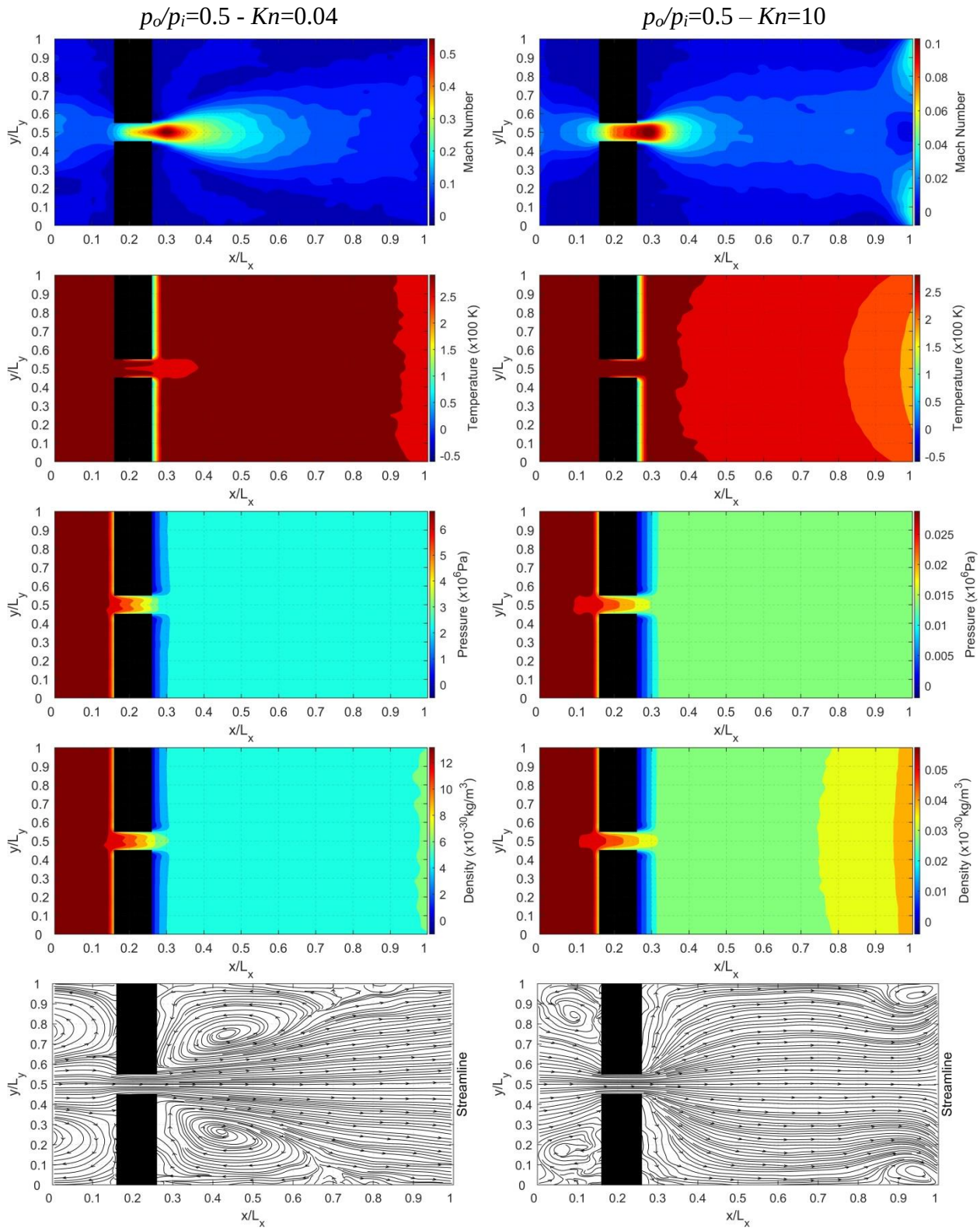

Figure 11 Contour plots of Mach number, Temperature, pressure, density and streamline. For H=500 - L=1000: p_o/p_i=0.5 - Kn=0.04(Left Column), p_o/p_i=0.5 - Kn=10(Right Column).

For Kn=0.04, H=1000 and L=0, pressure ratio p_o/p_i = 0.01-0.1-0.5 was applied in Figure 12. Increasing the pressure ratio by 100 times did not cause a big change in flow properties and Mach disc structure due to chocked flow. The most notable change in the contour plot is a slight increase in the length of the barrel shock along the channel. Changing the pressure ratio from p_o/p_i =

0.1 to 0.5, Mach number disproportionately doubled at the same Kn.

p_o/p_i for Kn=0.04

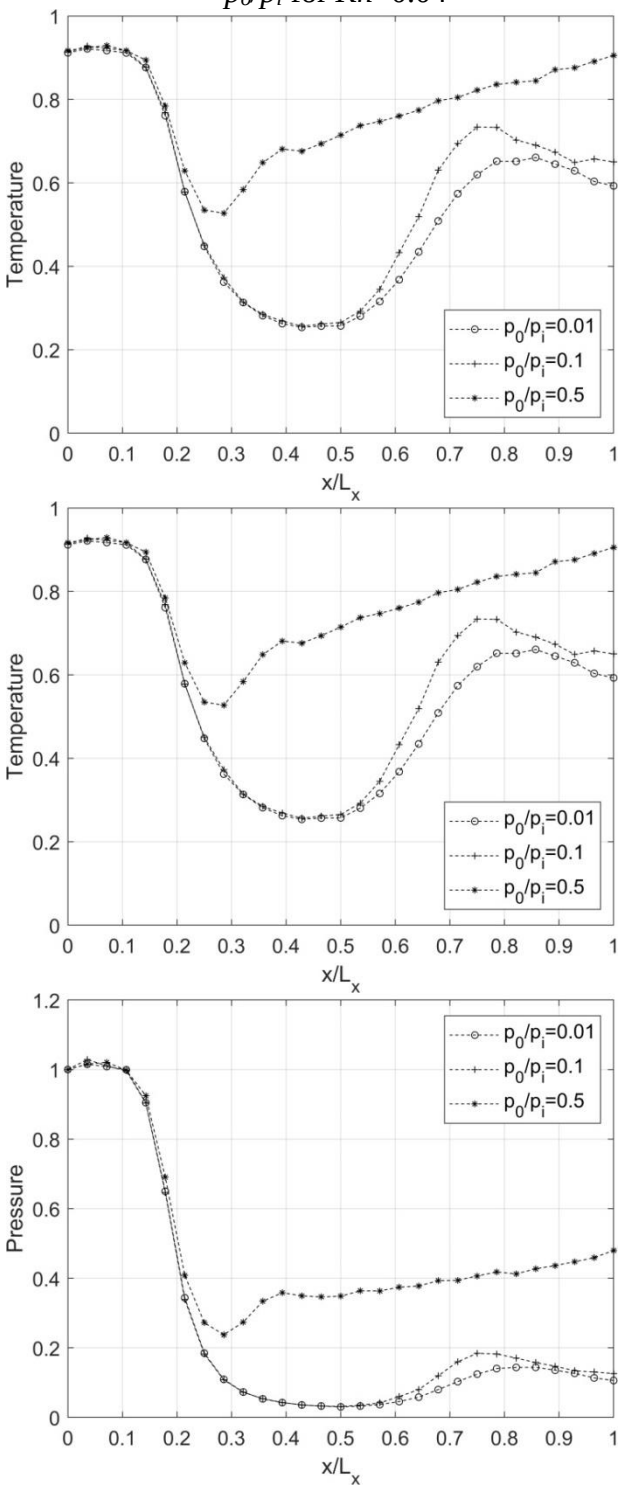

p_o/p_i=0.01

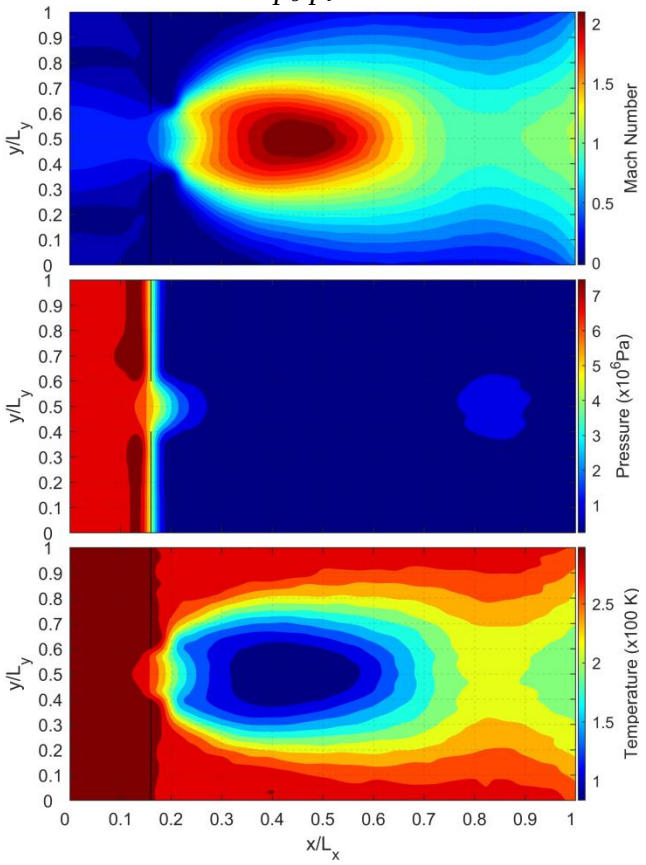

p_o/p_i=0.1

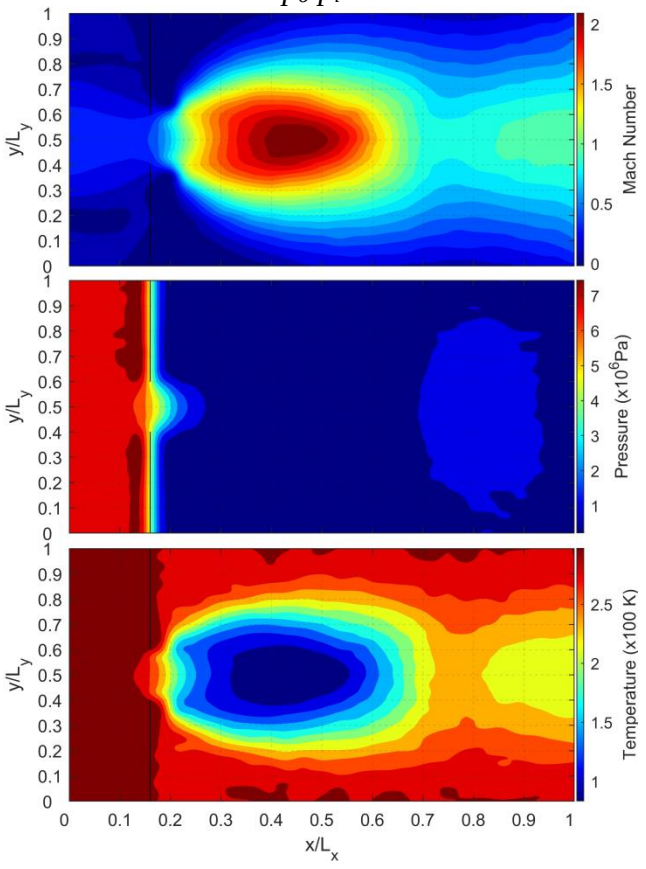

Figure 12 M, T and p distributions and contour plots depending on p_o/p_i for Kn=0.04, H=1000 and L=0. Top contour and bottom contour plots are p_o/p_i =0.01 and 0.1, respectively.

The enlargement of L reduced the pressure drop at the slit outlet. For H=250-500-1000, M, T and p distributions are given along the channel at Kn=0.04-10 in Figure 13. Fluctuation in the property distributions at the slit outlet is less at H=250. Thus, the settling of the flow properties was shorter at given Kn compared to high H. The positions of the Mach disc on the x-axis of the channel were similar to the study in Kn=0.01 [37]. However, the presence of plates and the difference in Kn caused sudden property changes at the slit outlet to be softer in EDMD.

In the distributions for some cases in this paper, the continuous decrease of the properties especially pressure and density from slit outlet to the channel outlet is because of low-pressure ratio is applied only to channel outlet.

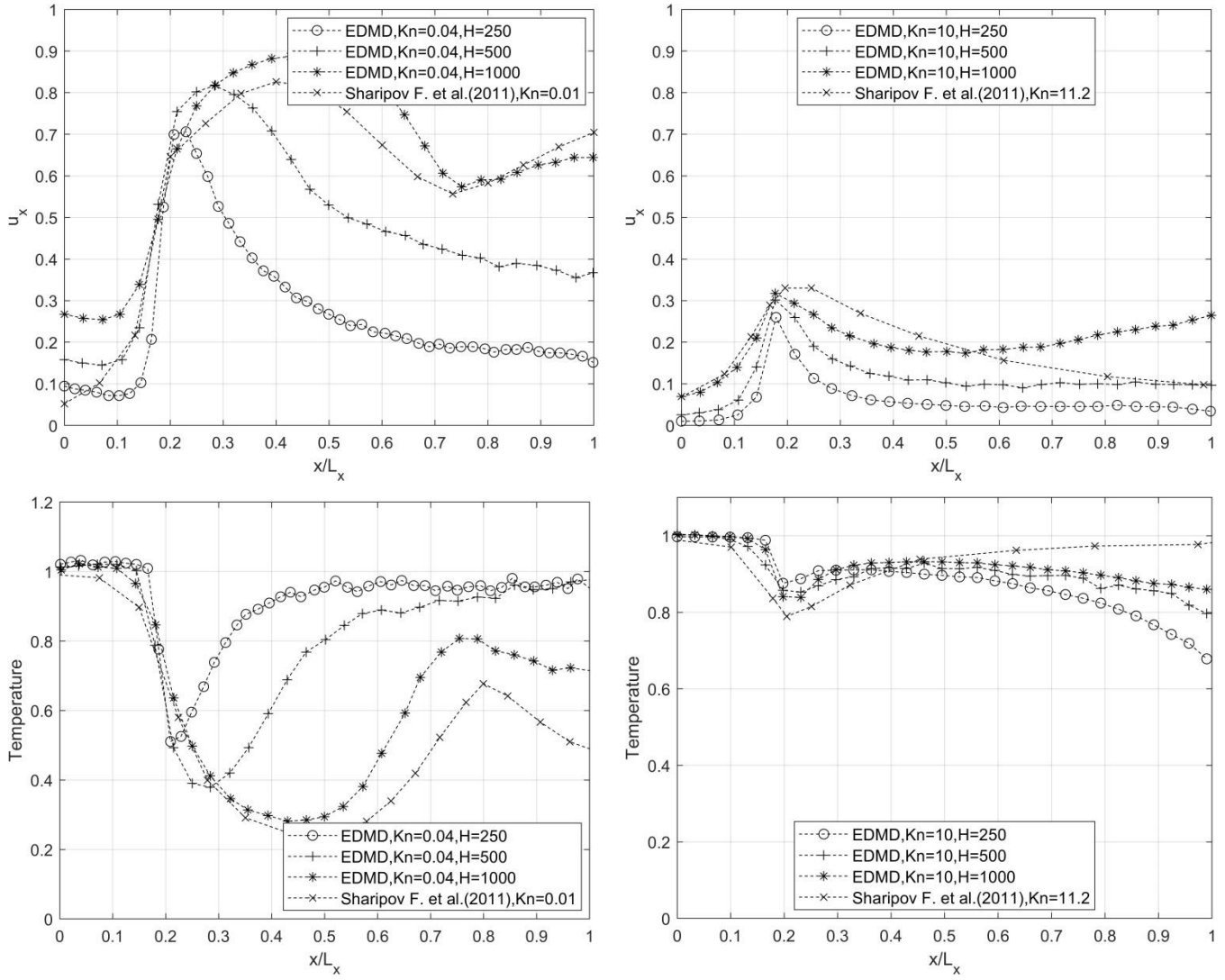

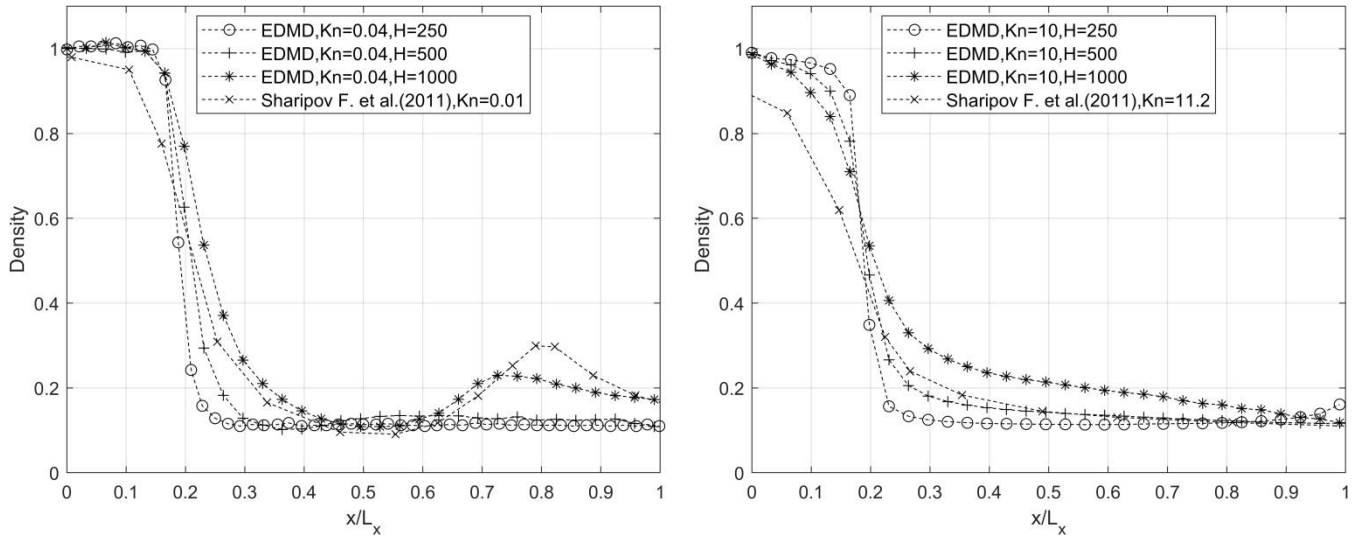

Figure 13 Distribution depending on *Kn* along L_x for dimensionless u_x, T and n. *Kn*=0.04(top) and *Kn*=10(bottom), p_o/p_i=0.1 for H=250, H=500 and H=1000 (L=0).

5. CONCLUSION

Effects of Kn and pressure ratio as well as H and L on the flow rate and flow property distributions along the channel have been investigated in the flow through a slit-type obstacle placed between two parallel plates. Simulations have been carried out for different cases, considering various L and H dimensions. The flow rate according to L/H ratio was examined in the transition regime and compared qualitatively with the literature.

Until the Kn number reaches the transition regime, the flow rate does not change significantly, but it decreases rapidly from the transition to the molecular regime. The flow rate typically increases as the pressure ratio increases for the same Kn. The difference between pressure ratios decreases as it approaches the steady state. While increasing the H increases the flow rate for high Kn, it has been observed that this difference decreases towards the continuous regime. While the increase in L/H ratio decreases the flow rate regardless of the pressure ratio and Kn, it has also been observed that it shifts the transition regime towards smaller Kn. In a case of different Kn, increasing of Kn results in increasing flow velocity. Because as Kn decreases, the inlet and outlet pressure difference (Δp) increases even if the pressure ratio remains constant.

Regardless of the pressure ratio, the formation of Mach discs is not observed as the flow regime passes from the continuous regime to the transition regime. For the same Kn in continuum regime, increasing the pressure ratio triggers the disc formation, but increasing the pressure ratio excessively will cause the flow to be chocked, and since the flow rate will no longer increase, there will be no serious change in the shape of the disc. Although the formation of Mach discs is directly dependent to Kn and the pressure ratio, H and L dimensions also play an important role for this phenomenon. For the same simulation case, an increase in H triggers disc formation, while an increase in L prevents disc formation as it decreases Mach and flow rate.

The characteristic of the vortices formed behind and in front of the slit is determined for different Kn, pressure ratio, H and L. Accordingly, it has been observed that increasing Kn decreases the size of the vortices and even almost loses and changes its position from the back of the slit (downstream direction) to the front (upstream direction). Although the H values given in the literature are not quantitatively specified, similar results were obtained at H=1000 according to the distribution data in the x-direction obtained for different H based on the L_y / H ratio. Thus, the effects of H and L variation on flow properties, streamlines and Mach disk structure are revealed independently of Kn and pressure ratio.

This study is important to understand vortices formation and shapes at inlet and outlet of the slit depending on Kn, pressure ratio and the slit gap geometry and showed that Mach disc, which is known to depend only on pressure ratio and Kn, can actually be controlled by H and L dimensions. It can also be important for controlling or measuring sudden pressure changes in similar applications.

Funding

The author (s) has no received any financial support for the research, authorship or publication of this study.

The Declaration of Conflict of Interest/ Common Interest

No conflict of interest or common interest has been declared by the authors.

Authors' Contribution

The authors contributed equally to the study.

The Declaration of Ethics Committee Approval

This study does not require ethics committee permission or any special permission.

The Declaration of Research and Publication Ethics

The authors of the paper declare that they comply with the scientific, ethical and quotation rules of SAUJS in all processes of the paper and that they do not make any falsification on the data collected. In addition, they declare that Sakarya University Journal of Science and its editorial board have no responsibility for any ethical violations that may be encountered, and that this study has not been evaluated in any academic publication environment other than Sakarya University Journal of Science.

REFERENCES

[1] P. J. Abbott, Z. J. Jabour, "Vacuum technology considerations for mass metrology," Journal of Research of the National Institute of Standards and Technology, vol. 116, no. 4, pp. 689–702, 2011.

[2] A. P. Polikarpov, I. Graur, "Unsteady rarefied gas flow through a slit," Vacuum, vol. 101, pp. 79–85, 2014.

[3] K. Jousten, S. Pantazis, J. Buthig, R. Model, M. Wüest, J. Iwicki, "A standard to test the dynamics of vacuum gauges in the millisecond range," Vacuum, vol. 100, pp. 14–17, 2014.

[4] S. Pantazis, D. Valougeorgis, "Rarefied gas flow through a cylindrical tube due to a small pressure difference," European Journal of Mechanics, B/Fluids, vol. 38, pp. 114–127, Mar. 2013.

[5] S. Varoutis, C. Day, F. Sharipov, "Rarefied gas flow through channels of finite length at various pressure ratios," Vacuum, vol. 86, no. 12, pp. 1952–1959, Jul. 2012.

[6] A. A. Alexeenko, D. A. Levin, S. F. Gimelshein, M. S. Ivanov, A. D. Ketsdever, "Numerical and experimental study of orifice flow in the transitional regime," 35th AIAA Thermophysics Conference, 2001.

[7] G. A. Bird, "Molecular gas dynamics and the direct simulation of gas flows," Oxford: Clarendon Press, 1994.

[8] I. Kandemir, "A multicell molecular dynamics method [Ph.D. thesis]," Case Western Reserve University, Cleveland, Ohio, USA, 1999.

[9] I. Greber, C. Sleeter, I. Kandemir, "Molecular dynamics simulation of unsteady diffusion," in AIP Conference Proceedings, Aug. 2001, vol. 585, pp. 396–400.

[10] V. R. Akkaya, I. Kandemir, "Event-driven molecular dynamics simulation of hard-sphere gas flows in microchannels," Mathematical Problems in Engineering, vol. 2015, 2015.

[11] B. J. Alder, T. E. Wainwright, "Phase transition for a hard sphere system," The Journal of Chemical Physics, vol. 27, no. 5. pp. 1208–1209, 1957.

[12] D. C. Rapaport, "The event scheduling problem in molecular dynamic simulation," Journal of Computational Physics, vol. 34, no. 2, pp. 184–201, 1980.

[13] A. Donev, A. L. Garcia, B. J. Alder, "Stochastic Event-Driven Molecular Dynamics," Journal of Computational Physics, vol. 227, no. 4, pp. 2644–2665, Feb. 2008.

[14] M. N. Bannerman, R. Sargant, L. Lue, "DynamO: A free O(N) general event-driven molecular dynamics simulator," Journal of Computational Chemistry, vol. 32, no. 15, pp. 3329–3338, Nov. 2011.

[15] G. A. Bird, "Molecular Gas Dynamics and the Direct Simulation of Gas Flows, " Oxford: Clarendon Press, 1994.

[16] G. D. Danilatos, "Direct simulation Monte Carlo study of orifice flow," in AIP Conference Proceedings, Aug. 2001, vol. 585, pp. 924–932.

[17] F. Sharipov, "Rarefied Gas Flow Through an Orifice at Finite Pressure Ratio," in AIP Conference Proceedings, Jun. 2003, vol. 663, pp. 1049–1056.

[18] F. Sharipov, "Numerical simulation of rarefied gas flow through a thin orifice," Journal of Fluid Mechanics, vol. 518, pp. 35–60, Nov. 2004.

[19] M. Wang, Z. Li, "Simulations for gas flows in microgeometries using the direct simulation Monte Carlo method," International Journal of Heat and Fluid Flow, vol. 25, no. 6, pp. 975–985, Dec. 2004.

[20] F. Sharipov, J. L. Strapasson, "Ab initio simulation of rarefied gas flow through a thin orifice," Vacuum, vol. 109, pp. 246–252, 2014.

[21] I. A. Graur, A. P. Polikarpov, F. Sharipov, "Numerical modelling of rarefied gas flow through a slit at arbitrary pressure ratio based on the kinetic equation," Zeitschrift fur Angewandte Mathematik und Physik, vol. 63, no. 3, pp. 503–520, Jun. 2012.

[22] A. R. Rahmati, R. Ehsani, "Simulation of Micro-Channel and Micro-Orifice Flow Using Lattice Boltzmann Method with Langmuir Slip Model," Nano Micro Scales, vol. 5, no. 1, pp. 1–8, 2017.

[23] J. Zhang, "Lattice Boltzmann method for microfluidics: Models and applications," Microfluidics and Nanofluidics, vol. 10, no. 1. Springer Verlag, pp. 1–28, Jan. 01, 2011.

[24] S. Misdanitis, S. Pantazis, D. Valougeorgis, "Pressure driven rarefied gas flow through a slit and an orifice," Vacuum, vol. 86, no. 11, pp. 1701–1708, May 2012.

[25] P. L. Bhatnagarp, E. P. Gross, A. M. Krook, "Model for Collision Processes in Gases. I. Small Amplitude Processes in Charged and Neutral One-Component Systems~," 1954.

[26] S. F. Gimelshein, G. N. Markelov, T. C. Lilly, N. P. Selden, A. D. Ketsdever, "Experimental and numerical modeling of rarefied gas flows through orifices and short tubes," in AIP Conference Proceedings, May 2005, vol. 762, pp. 437–443.

[27] C. T. Lilly, F. S. Gimelshein, D. A. Ketsdever, N. G. Markelov, "Measurements and computations of mass flow and momentum flux through short tubes in rarefied gases," Physics of Fluids, vol. 18, no. 9, 2006.

[28] J. Lindström, J. Bejhed, J. Nordström, "Measurements and numerical modelling of orifice flow in microchannels," 41st AIAA Thermophysics Conference, 2009.

[29] F. Sharipov, "Transient flow of rarefied gas through an orifice," Journal of Vacuum Science & Technology A: Vacuum, Surfaces, and Films, vol. 30, no. 2, p. 021602, Mar. 2012.

[30] M. T. Ho, I. Graur, "Numerical study of unsteady rarefied gas flow through an

orifice," Vacuum, vol. 109, pp. 253–265, 2014.

[31] A. L. Garcia, W. Wagner, "Generation of the Maxwellian inflow distribution," Journal of Computational Physics, vol. 217, no. 2, pp. 693–708, Sep. 2006.

[32] G. Paul, "A Complexity O(1) priority queue for event driven molecular dynamics simulations," Journal of Computational Physics, vol. 221, no. 2, pp. 615–625, Feb. 2007.

[33] M. Marín, P. Cordero, "An empirical assessment of priority queues in event-driven molecular dynamics simulation," Computer Physics Communications, vol. 92, no. 2–3, pp. 214–224, 1995.

[34] W. W. Liou, Y. C. Fang, "Implicit boundary conditions for direct simulation Monte Carlo method in MEMS flow predictions," CMES - Computer Modeling in Engineering and Sciences, 2000.

[35] M. Koc, I. Kandemir, V. R. Akkaya, "An Investigation of Transition Flow in Porous Media by Event Driven Molecular Dynamics Simulation," Journal of Applied Fluid Mechanics, vol. 14, no. 1, pp. 23–36, 2020.

[36] S. Varoutis, O. Sazhin, D. Valougeorgis, and F. Sharipov, "Rarefied gas flow into vacuum through a short tube," 51st IUVSTA Workshop on Modern Problems and Capability of Vacuum Gas Dynamics.

[37] F. Sharipov, D. V. Kozak, "Rarefied gas flow through a thin slit at an arbitrary pressure ratio," European Journal of Mechanics, B/Fluids, vol. 30, no. 5, pp. 543–549, Sep. 2011.